Elusive intermediates in cisplatin reaction with target amino acids: platinum(II)-cysteine complexes assayed by IR ion spectroscopy and DFT calculations

Davide Corinti[a,+]*, Roberto Paciotti[b,+,]**, Cecilia Coletti[b], Nazzareno Re[b], Barbara Chiavarino[a], Maria Elisa Crestoni[a], Simonetta Fornarini[a]

[a] Dipartimento di Farmacia, Università G. D'Annunzio Chieti-Pescara, Via dei Vestini 31, Chieti I-66100, Italy

[b] Dipartimento di Chimica e Tecnologie del Farmaco, Università di Roma "La Sapienza", I-00185 Roma, Italy

*davide.corinti@uniroma1.it; **r.paciotti@unich.it

[+]The authors contributed equally.

Abstract

The reactivity of a widely used inorganic antineoplastic drug, cisplatin, *cis*-$PtCl_2(NH_3)_2$, with L-cysteine (Cys) has been investigated using a combination of electrospray ionization mass spectrometry (ESI-MS), IR ion spectroscopy and DFT calculations. The lateral chain of cysteine represents one of the main platination sites in proteins, a process often invoked among the resistance mechanisms of cancer cells to cisplatin. ESI-MS has allowed the identification of several ionic species derived from the interaction of both cisplatin and its active hydrolized form, *cis*-$[PtCl(NH_3)_2(H_2O)]^+$, with cysteine. Among them, the mass-selected substitution product *cis*-$[PtCl(NH_3)_2(Cys)]^+$ and the formally pentacoordinated complex *cis*-$[PtCl(NH_3)_2(H_2O)(Cys)]^+$ were assayed by IR ion spectroscopy. The recorded vibrational features were compared to DFT-calculated IR spectra eventually assessing the structures of the sampled ions. In *cis*-$[PtCl(NH_3)_2(Cys)]^+$ cysteine was found to bind platinum through the sulfur atom as a thiolate zwitterion, thus highlighting the augmented acidity of the cysteine thiol group after metal coordination. On the other hand, the *cis*-$[PtCl(NH_3)_2(H_2O)(Cys)]^+$ structure was found to comply with a non-covalent adduct of the charged active species *cis*-$[PtCl(NH_3)_2(H_2O)]^+$ with neutral cysteine. This complex is

able to undergo at substitution process to produce *cis*-$[PtCl(NH_3)_2(Cys)]^+$ when activated as a mass-isolated ion, suggesting its participation in the reaction mechanism of cisplatin with cysteine in solution. Finally, the DFT-calculated energy profile for the substitution reaction was correlated with the peculiar gas-phase reactivity of this non-covalent complex, which showed to be 10-fold less reactive towards substitution than the corresponding methionine complex. Calculations agree in indicating slower kinetics for this reaction, despite a similar energy balance in the overall exoergonic process, in agreement with cisplatin affinity towards thiol-containing molecules.

Graphical abstract

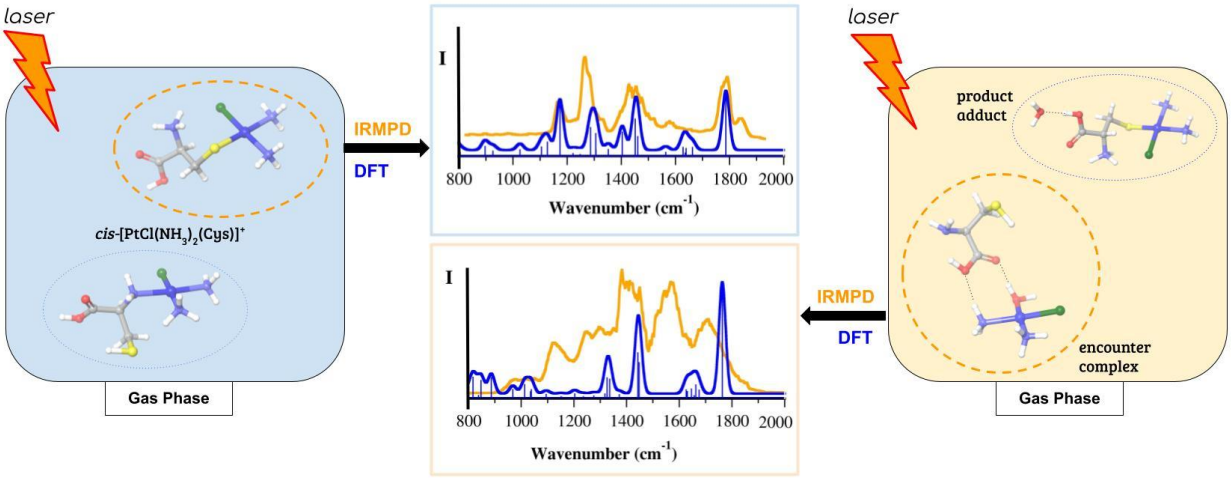

Cisplatin reaction with cysteine leads to the formation of the substitution product *cis*-$[PtCl(NH_3)_2(Cys)]^+$, the structure of which was unveiled by IRMPD spectroscopy and DFT calculations. Details on the mechanism and kinetic of the substitution reaction were obtained from the characterization and activation of the encounter complex *cis*-$[PtCl(NH_3)_2(H_2O)(Cys)]^+$.

Keywords

Antineoplastic drug; platinum complex; ligand substitution mechanism; structural characterization; IR laser spectroscopy; mass spectrometry

1. Introduction

Cisplatin, *cis*-diamminedichloroplatinum(II), *cis*-$PtCl_2(NH_3)_2$, is an antineoplastic drug which still represents the core therapeutic for the treatment of several solid tumors including neck, lung and prostate cancers. Its activity is based on the interaction with nitrogen-containing bases of DNA. C isplatin can undergo spontaneous hydrolysis followed by water or hydroxyl substitution by the N7 atom of guanine, ultimately leading to the formation of 1,2-intrastrand crosslinks. The DNA morphology is thus disrupted, eventually hindering transcription and replication of the genetic information [1-6]. Cisplatin, however, does not interact only with nucleic acids in the biological media. Several evidences have shown the importance of protein and peptide binding for the distribution and inactivation of the drug [7]. Sulfur-containing aminoacidic residues, such as methionine and cysteine, represent cisplatin favorite binding sites together with the nitrogen atom of the imidazole group of histidine, in agreement with the soft acid character of Pt(II) [8-19]. In a combined effort to obtain a detailed characterization of the binding motifs of platinum/peptide interactions, we have reported on the interaction of cisplatin with the L-histidine and L-methionine proteinogenic amino acids using an integrated approach of experimental techniques, namely electrospray ionization mass spectrometry (ESI-MS) and IR multiple photon dissociation (IRMPD) spectroscopy, backed by quantum-mechanics calculations [20-23]. Mass isolation and vibrational characterization of *cis*-$[PtCl(NH_3)_2(L)]^+$, where L stands for either L-methionine or L-histidine, have unambiguously shown the preferential coordination of Pt to the sulfur atom of methionine and to the imidazole N atom of histidine, respectively. The use of IRMPD spectroscopy has demonstrated to be particularly effective to provide structural information on the substitution product of cisplatin not only with amino acids, but also with

nucleobases and nucleotides [20-29]. This powerful technique allows to obtain the IR spectra of mass selected ions by monitoring their dissociation yield when interacting with the light of a tunable IR laser [30-34]. IRMPD spectra are not influenced by matrix effects and can be directly compared to theoretical IR spectra for vibrational mode assignment and structural elucidation of the sampled ion population. Our scientific interest has also focused on the cisplatin substitution reaction for both mechanistic and kinetic features. Mass spectrometry gives the unique possibility to select and isolate, from the complex mixture of species generated by hydrolysis of cisplatin, the most active intermediate in the cell media, i.e. the aquacomplex *cis*-$[PtCl(NH_3)_2(H_2O)]^+$ and to assay its structural and reactivity features [1,5,6,35,36]. The reaction efficiencies for the substitution of the water molecule from both *cis*-$[PtCl(NH_3)_2(H_2O)]^+$ and the doubly aquated complex *cis*-$[Pt(NH_3)_2(OH)(H_2O)]^+$ with neutral volatile ligands modeling biological functionalities were obtained by performing ion-molecule reactions in the cell of a FT-ICR mass spectrometer, finding the former complex to be more reactive toward substitution [37]. Obtaining clear experimental results on the efficiencies for the reaction of *cis*-$[PtCl(NH_3)_2(H_2O)]^+$ with aminoacids or even more complex biomolecules is indeed a hard task considering their low volatility. Incidentally, a strategy to obtain semi-quantitative data on the reactivity of the aqua complex of cisplatin with amino acids was found by examining the species generated by ESI-MS of solutions containing the chosen ligand (L) and cisplatin. Formally pentacoordinated complexes with the general formula *cis*-$[PtCl(NH_3)_2(H_2O)(L)]^+$ can in fact be observed and isolated [23,38,39]. IRMPD spectroscopy identified these species as the encounter complex for the substitution reaction in solution following the Eigen-Wilkins model [40,43]. When activated, these complexes show two main fragmentation channels, i.e., water and L loss, which appear in different ratios depending on the nature of the ligand and can be directly related to the reaction efficiencies for substitution. A similar experimental protocol, comprising the activation of mass-selected non-covalent Pt(IV)

complexes with ascorbate, allowed the identification of specific structural motifs involved in the faster reduction kinetics of Pt(IV) complexes with axial hydroxido ligands when compared to complexes with axial acetato ligands in the presence of ascorbic acid [44]. IRMPD spectroscopy was also employed to determine the structural features of cysteine complexes with alkali metal cations and divalent metals [45-47]. Binding motifs were found to differ based on the nature of the metal and on the influence of the charge location on the amino acid [45-49]. Cysteine radical ions were also examined with the same technique [50-52], because of the importance of the equilibrium between cysteine and the disulfide dimer cystine to maintain the redox homeostasis in living cells [53-55].

In the present contribution this combined methodology is applied to detail the reactivity of cisplatin toward the natural amino acid L-cysteine. The primary ligand substitution complex, *cis*-$[PtCl(NH_3)_2(Cys)]^+$, has been characterized using IRMPD spectroscopy and DFT calculations, confirming the preferential binding of platinum to the sulfur atom. Interestingly, spectroscopy highlights the sole existence of cysteine in zwitterionic form when platinated, confirming an increase of acidity of the Pt-thiol functionality when compared to bare thiols. Structure and dissociation of the encounter complex, *cis*-$[PtCl(NH_3)_2(H_2O)(Cys)]^+$, have eventually been explored. The geometry assigned to the assayed population shows an external neutral cysteine bound to the cisplatin aqua complex, in agreement with the notion that the deprotonation of the cysteine thiol group is activated by platination. Activation of the complex produces an unusually low percentage of water loss (ca. 75%) when compared to the methionine case (ca. 97%) [23] suggesting a higher activation threshold for the substitution reaction with the thiol-containing amino acid cysteine. Theoretical assessment of this experimental evidence has been obtained through the characterization of the potential energy surface of the substitution reaction.

2. Methods

2.1 Sample preparation and MS analysis

Both cisplatin and L-cysteine were acquired from commercial source (Sigma Aldrich) and used as received. L-cysteine and cisplatin were solubilized in water, each one at a concentration of 10^{-3} M, and finally mixed and diluted in water/methanol 1:1. The final concentration of the so obtained solution was 10^{-5} M. To enhance the signal of the positively charged complexes generated by reaction of cisplatin with cysteine, formic acid was added to the solution to a final concentration of 3×10^{-5} M.

2.2 IRMPD spectroscopy

Two frequency ranges, namely 800-2000 cm^{-1} and 3100-3700 cm^{-1}, were explored to obtain IRMPD spectra of both *cis*-$[PtCl(NH_3)_2(Cys)]^+$ and *cis*-$[PtCl(NH_3)_2(H_2O)(Cys)]^+$ employing two experimental setups, both involving an ion trap mass spectrometer coupled with the beamline of a tunable IR laser. The "fingerprint" range, 800-2000 cm^{-1}, was assayed using the light of the Centre Laser Infrarouge d'Orsay (CLIO) free electron laser (FEL), delivered on ions trapped in a hybrid FT-ICR tandem mass spectrometer (APEX-Qe Bruker Daltonics)[56], equipped with a 7.0 T actively shielded magnet. This instrument presents a quadrupole/hexapole interface for mass selection and accumulation. Ions were accumulated for 1.0 s in the hexapole, containing argon as buffer gas, in order to cool them prior to their transfer into the ICR cell where they were irradiated with the IR FEL light for either 300 or 500 ms (on *cis*-$[PtCl(NH_3)_2(Cys)]^+$ and *cis*-$[PtCl(NH_3)_2(H_2O)(Cys)]^+$, respectively) and the photofragmentation products mass analyzed. The FEL radiation is delivered in trains of 9 μs long macropulses at a repetition rate of 25 Hz. A macropulse comprises 600 micropulses, each few ps long. The FEL electron energy was set at 42.3 MeV and the average laser power was 1200 mW corresponding to a macropulse energy of 50 mJ. The 3100-3800 cm^{-1} range, which comprises the X-H (X = C, N, O) stretching modes, was recorded on a modified ion trap mass

spectrometer (Bruker Esquire 6000) adapted to be coupled with an optical parametric oscillator/amplifier laser (OPO/OPA, LaserVision, Bellevue, WA, U.S.A) [57]. The 1064 nm fundamental of a Nd:YAG laser (Continuum Surelite II) operating at 9 Hz repetition powers this system which generates a typical output energy of ca. 19 mJ/pulse in the spectral range of investigation with 3 - 4 cm^{-1} bandwidth. In the ion trap, ions are accumulated for 20-50 ms, mass selected and submitted to irradiation for a time lapse ranging from 0.5 to 1 s. The laser wavelength was continuously changed at a speed of 0.1 cm^{-1} s^{-1}.

In both ranges, the mass spectrum was obtained from an accumulation over 4 scans.

To obtain the IR action spectra, the photofragmentation yield $R = -\ln[I_p/(I_p + \Sigma I_f)]$, where I_p and ΣI_f are the parent and sum of the fragment ion intensities, respectively, is plotted as a function of the radiation wavenumber [58].

2.3 Computational details

The lowest energy conformations of the primary association complex *cis*-$[PtCl(NH_3)_2(Cys)]^+$ and of the encounter complex *cis*-$[PtCl(NH_3)_2(H_2O)(Cys)]^+$ were identified by performing a computational search at the semiempirical tight-binding level, adopting the iMTD-GC approach implemented in CREST [59]. In particular, the iMTD-GC algorithm generates conformer/rotamer ensembles (CREs) by performing an extensive metadynamic sampling (MTD) with an additional genetic z-matrix crossing (GC) step. For each complex, the representative structures were minimized at the B3LYP/6-311+G(d,p) level of theory, using the LANL2DZ pseudopotential for platinum. Then, a visual inspection was performed to identify possible conformers that might have escaped from the conformational search. Electronic energies, thermodynamic properties (zero point energy (ZPE), thermal corrections, and entropies), and harmonic frequencies were calculated by minimizing the selected structures at the B3LYP level of theory using a combined basis set,

hereafter indicated as BS1, consisting of the 6-311+G(3df) basis set for the sulfur atom and 6-311+G(2df,pd) for the remaining atoms, except platinum, for which the LANL2TZ-f pseudopotential was adopted. The relative energies of the investigated complexes were also computed at the ωB97X-D/BS1//B3LYP/BS1 level of theory to include the effects of long-range interactions in the energetics. Harmonic frequencies computed for *cis*-$[PtCl(NH_3)_2(H_2O)(Cys)]^+$ and *cis*-$[PtCl(NH_3)_2(Cys)]^+$ complexes, in the 800−2000 and 2800−3800 cm^{-1} ranges, were scaled by 0.990 and 0.957, respectively. All the calculated spectra were convoluted assuming a Gaussian profile with an associated width (fwhm) of 15 cm^{-1} in the 800−2000 cm^{-1} range and 5 cm^{-1} in the 2800−3800 cm^{-1} frequency range. All quantum chemical calculations were performed using the Gaussian 09 package [60].

3. Results and discussions

3.1 Platination of cysteine: positively charged intermediates

Cisplatin readily forms complexes with cysteine when the two species are allowed to interact in a methanol/water solution which favors the aquation of cisplatin. Using ESI-MS, ions generated in solution can be revealed and assayed in the gas-phase allowing a direct sampling of the ionic species. Furthermore, MS-based techniques can be exploited for structural characterization. Fig. S1 reports the mass spectrum of the cisplatin/cysteine solution in which three major clusters of signals presenting the typical isotopic pattern of Pt combined with a Cl atom appear at *m/z* 384-388, 402-406 and 420-424. To simplify the forthcoming discussion, ions containing Pt and Cl will be defined by the isotopic signal containing ^{194}Pt and ^{35}Cl, thus we will refer to ions at *m/z* 384, 402 and 420. The first in the series is consistent with the formula *cis*-$[PtCl(NH_3)_2(Cys)]^+$. Cysteine has substituted a chlorine atom of cisplatin leading to a positively charged species. The photofragmentation pathway (Fig. S2) agrees with the attribution, showing fragments at *m/z* 367,

350 and 331 generated from neutral losses consistently found in substitution products of cisplatin (assigned to NH_3, $2NH_3$ and NH_4Cl losses, respectively) [20-22,24,28].

The ion at *m/z* 402, the formally pentacoordinated complex *cis*-$[PtCl(NH_3)_2(H_2O)(Cys)]^+$, can be attributed to the encounter complex of aquated cisplatin with neutral cysteine. {*cis*-$[PtCl(NH_3)_2(H_2O)]^+ \cdot (Cys)$}, on the basis of the structural and spectroscopic characterization of similar platinum complexes presenting various external ligands, e.g., methionine, 4-methylimidazole, acetamide, etc. [23,38,39]. An accurate description of the structural features of this ion will be discussed in Section 3.3. Its photodissociation, shown in Fig. S3, occurs by loss of neutral water and by loss of cysteine (*m/z* 384 and 281, respectively) in a similar fashion as already observed in previous reports on cisplatin-derived encounter complexes [23,38,39]. The ratio between the two fragmentation paths was found to be correlated to the kinetics of the substitution reaction, as demonstrated by ion-molecule reactions observed with more volatile neutrals [38]. This finding is related to the nature of the pentacoordinated complex which models the first intermediate in the substitution process in solution following the Eigen-Wilkins reactant preassociation mechanism [40-43]. The extent of water loss is thus governed by the difference between threshold for the dissociation of non-covalently bound cysteine and the energy of the pentacoordinated transition state which leads to cysteine substitution of the water molecule, promptly followed by H_2O departure to form the final substitution complex (Scheme 1).

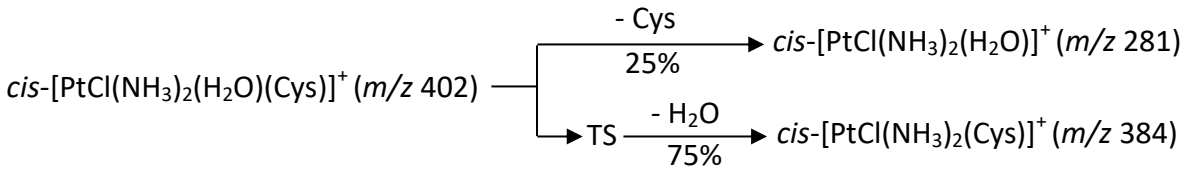

Scheme 1. Primary fragmentation channels of the *cis*-$[PtCl(NH_3)_2(H_2O)(Cys)]^+$ complex.

In the case of *cis*-$[PtCl(NH_3)_2(H_2O)(Cys)]^+$, the water loss channel (calculated including in the sum the abundances of ions formed in consecutive dissociation events, i.e. loss of ammonia) is 75% of

the total. This value is appreciably lower than the value observed in the photofragmentation of *cis*-$[PtCl(NH_3)_2(H_2O)(Met)]^+$ where water loss was largely predominant (ca. 97% of the total dissociation)[37]. This result suggests the kinetics for the *cis*-$[PtCl(NH_3)_2(H_2O)]^+$ substitution reaction to be slower for cysteine when compared to methionine. Finally, the *m/z* 420 ion can be attributed to a non-covalent complex of cisplatin with cysteine, *cis*-$[PtCl_2(NH_3)_2(Cys)H]^+$. The isotopic pattern is indeed consistent with the presence of two chlorido ligands (Fig. S4). Dissociation occurs by progressive loss of HCl and NH_3, together with protonated cysteine formed by direct departure of the aminoacid from the adduct with the platinum complex. Structural characterization of this ion is not reported here because the aquacomplex of cisplatin, the active species of interest in the biological media [1,5], is not involved in this instance.

3.2 IRMPD spectroscopy and structure of the substitution product cis-$[PtCl(NH_3)_2(Cys)]^+$

Cysteine can replace the water molecule from *cis*-$[PtCl(NH_3)_2(H_2O)]^+$ leading to the substitution complex *cis*-$[PtCl(NH_3)_2(Cys)]^+$ whereby cysteine may bind the metal via -SH, -NH_2 or -CO(OH) nucleophilic sites. Thus, we can postulate SH-, N- and O-platinated complexes of *cis*-$[PtCl(NH_3)_2(Cys)]^+$, hereafter referred to as **cSH**, **cN** and **cOH**, respectively. Moreover, both the SH and COOH functions can undergo deprotonation when covalently bound to Pt^{2+}. In this state, the acidity of SH/OH increases and the proton can move to the NH_2 group. In this configuration, cysteine assumes a formal zwitterionic state, here named **cSz** and **cOz,** where deprotonation involves the SH and COOH functions, respectively.

QM calculations were performed in the gas-phase to identify the most stable isomers and conformers of *cis*-$[PtCl(NH_3)_2(Cys)]^+$. The lowest energy structures of cis-$[PtCl(NH_3)_2(Cys)]^+$ isomers, namely **cSz-1**, **cSz-2**, **cSz-3** and **cSz-4**, are shown in Fig. 1. They are members of the S-platinated family with a protonated amino group. As a consequence, the NH_3^+ function can form three H bonds with the carboxylic C=O group and with S and Cl atoms. In the case of **cSz-1**, these contacts

reach the lowest distance values of 2.41, 2.26 and 2.07 Å for r(NH_2-H^+···Cl), r(NH_2-H^+···S) and r(NH_2-H^+···O=C), respectively. The 180° rotation of the COOH function in **cSz-4** (at 10.6 kJ mol^{-1} relative energy) leads to the formation of a NH_2-H^+···OH hydrogen bond and a consequently free C=O group.

In **cSz-2** and **cSz-3** the spatial disposition of COOH and NH_3^+ groups is similar to the one depicted in **cSz-1**, preserving all H bonds though characterized by longer distances.

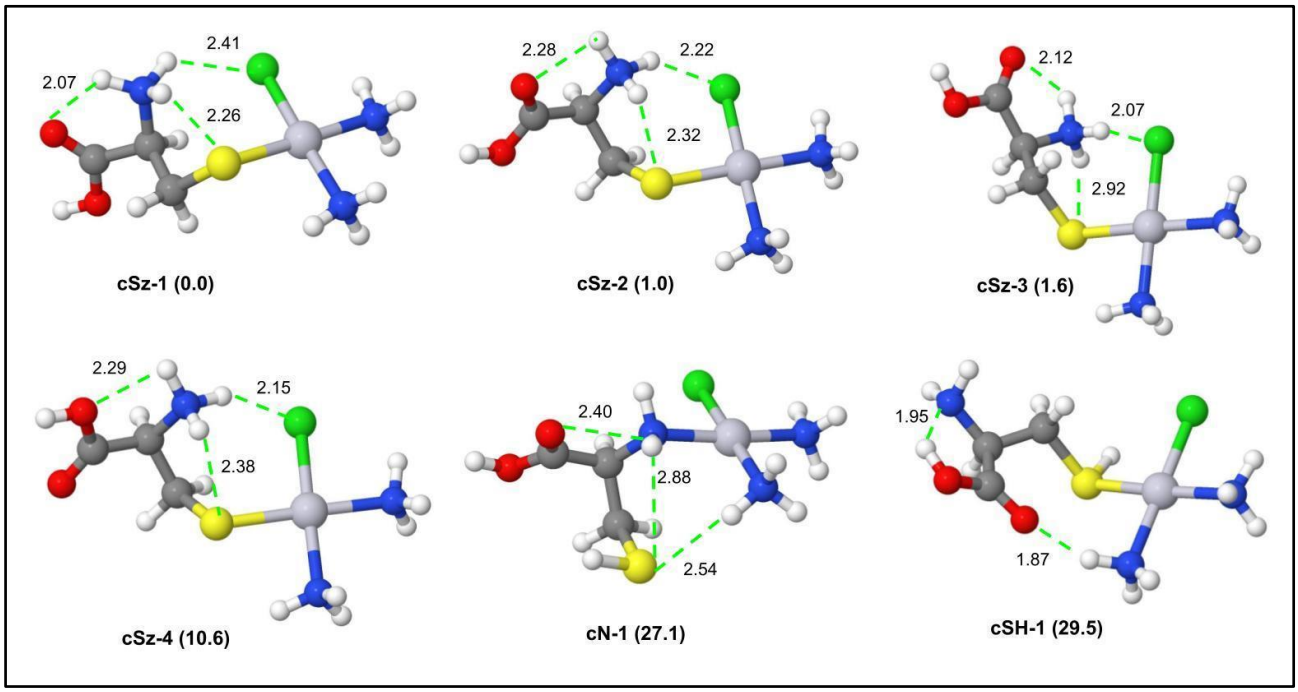

Fig. 1. Optimized geometries of the most stable conformers of the *cis*-$[PtCl(NH_3)_2(Cys)]^+$ ion, computed in gas phase at B3LYP/BS1 level of theory. Free energies relative to **cSz-1** are reported in parenthesis in kJ mol^{-1}. Hydrogen bond distances (Å) are indicated by green dashed lines.

In S-Pt adducts, i.e. **cSz-10** (57.4 kJ mol^{-1}) and **cSz-11** (78.2 kJ mol^{-1}), the proton transfer involves the C=O moiety as H^+ acceptor leading to a protonated carboxyl function $CO_2H_2^+$ (Fig. S5).

A different hydrogen bond pattern was observed in the SH-Pt derivatives. In the **cSH-1** isomer (29.5 kJ/mol) the amino nitrogen can establish a hydrogen bond with the H atom of the carboxylic function in *trans* configuration. The C=O group is involved in a H bond with the ammonia ligand. Notably, the **cSH** isomers are the only species where the α-NH_2 group can act as H bond acceptor

from the NH_3 ligand as in **cSH-2** (Fig. S6). The proton transfer from (Pt-bound)SH to α-NH_2 is characterized by a calculated free energy barrier of 9.1 kJ mol^{-1} (Fig. S7), suggesting that this process is not only thermodynamically favored but should also occur rapidly in the gas phase.

The lowest energy N-platinated isomer, **cN-1**, was found to lie at 27.1 kJ mol^{-1} relative energy, suggesting that the main isomer in the gas phase is S-platined, as previously found for *cis*-$[PtCl(NH_3)_2(Met)]^+$ [20]. In **cN-1** the S atom establishes two H bonds with NH_3 and NH_2 while the COOH group in *trans* configuration interacts with NH_2 via a C=O···H_2N contact. We also explored the conformational space of the O-platinated isomers (Fig. S5). The most stable members of this family, **cOz-1** and **cOH-1**, are characterized by a significant relative free energy (44.2 and 67.2 kJ mol^{-1}, respectively), indicating that the O-Pt derivatives are unlikely found in the present experimental conditions. Other optimized structures of isomers and conformers of *cis*-$[PtCl(NH_3)_2(Cys)]^+$ ion are shown in Fig. S5 and S6 while their relative free energy values are reported in Table S1. The substitution complex *cis*-$[PtCl(NH_3)_2(Cys)]^+$ was assayed by IRMPD spectroscopy, allowing the characterization of the vibrational and structural features of the ion (Fig. 2). The XH stretching region shows a strong absorption at 3563 cm^{-1} and a few smaller bands between 3400 and 3200 cm^{-1}. The fingerprint range of the IR spectrum presents several features. Particularly interesting is the presence of two bands around 1800 cm^{-1} where CO stretching modes usually absorb, suggesting two or more isomers to participate in the sampled population. Comparison with calculated IR spectra confirms this hypothesis. The experimental spectrum is well simulated by a combination of the vibrational modes computed for isomers in which cysteine, in zwitterionic form, is bound to Pt (Fig. 1) through the deprotonated thiolate functionality, while the protonated amino group interlaces multiple H-bond interactions. Interaction with Pt(II) is therefore activating the deprotonation of cysteine thiol, a process that is not relevant in the deprotonated cysteine ion nor in the zwitterion form of neutral cysteine at room temperature

[48,61]. Geometries corresponding to isomers/conformers **cSz-1** to **cSz-6** may play a role in the assayed population on account of both thermodynamic and spectroscopic data, on the basis of the tabulated energies in Table S1 and of the calculated spectra reported in Fig. S8-S11. However, in interpreting the IRMPD spectrum we will refer to the lowest lying isomers **cSz-1** and **cSz-2** together with **cSz-4** which accounts for a minor feature at 1800 cm^{-1}. Fig. 2 reports a comparison of the IRMPD spectrum with calculated ones, while vibrational assignments are reported in Table S2.

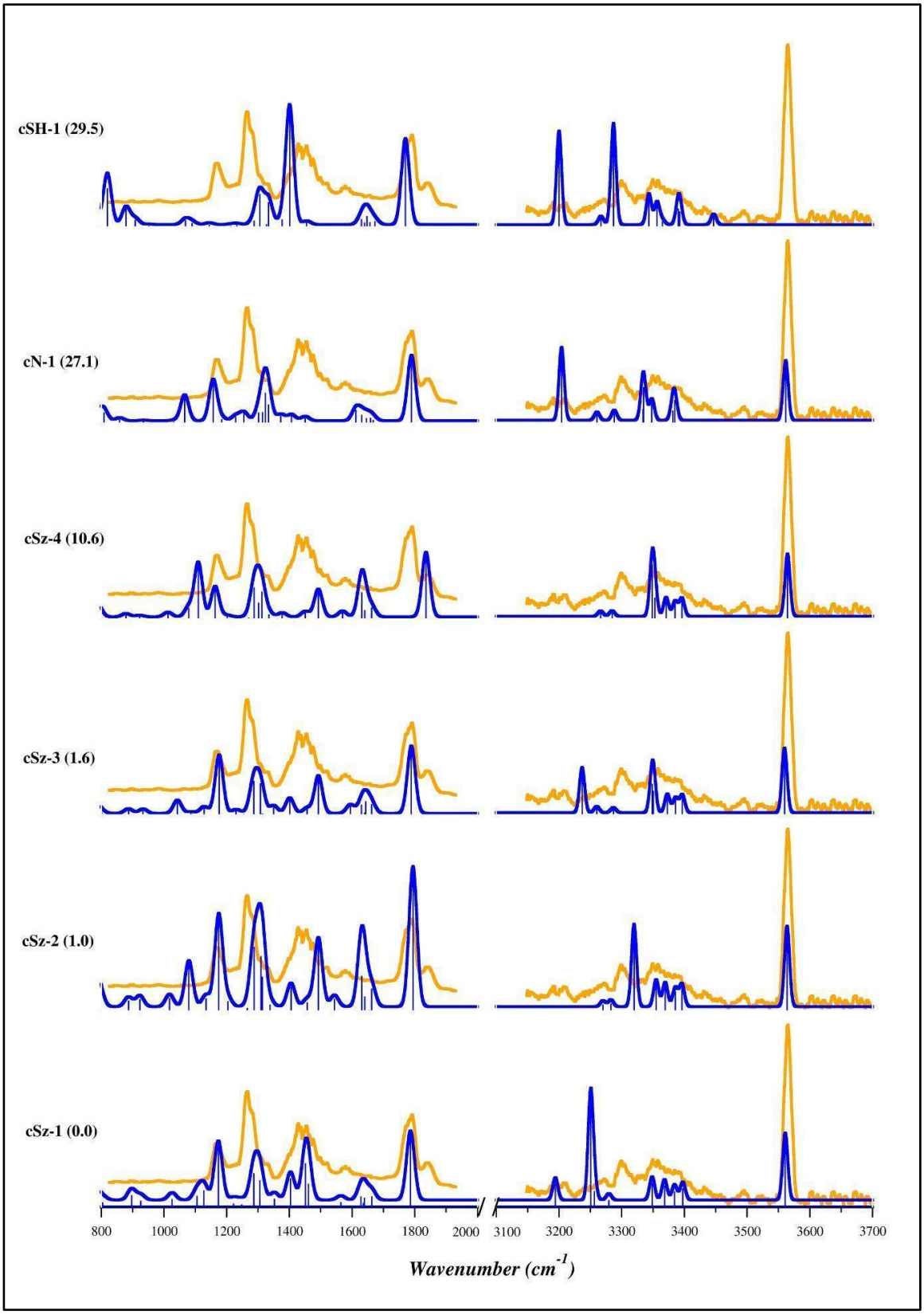

Fig. 2. IRMPD spectrum (orange profile) and calculated harmonic IR spectra (blue profiles) of the lowest lying conformers and isomers of *cis*-$[PtCl(NH_3)_2(Cys)]^+$ ion, computed at the B3LYP/BS1 level of theory. Free energies relative to **cSz-1** are reported in brackets (kJ mol^{-1}).

The sharp 3563 cm^{-1} band is interpreted by the OH stretching mode calculated at ca. 3562 cm^{-1} for the whole set of conformers in which cysteine is bound as a thiolate zwitterion. The several smaller features in the XH stretching range can be attributed to the symmetric and antisymmetric stretching modes of the ammonia ligands and of the NH_3^+ group of cysteine. The two bands at 1840 and 1793 cm^{-1} are in agreement with the CO stretching modes of **cSz-4** (1835 cm^{1}) and **cSz-1/2** (1786 and 1794 cm^{-1}), respectively. Indeed, the CO group of the former structure is only interacting with the *syn* carboxylic OH, while in **cSz-1** and **cSz-2** the carbonyl group is involved as H-bond acceptor with the protonated amino group, leading to a red-shift of its stretching frequency. In agreement with the lower intensity of the 1840 cm^{-1} experimental band, **cSz-4** is higher in energy by 10.4 kJ mol^{-1} (and presumably lower in relative abundance) compared with the lowest lying structure **cSz-1** (Fig. 2). The strong vibrational signature at 1453 cm^{-1} is particularly informative: it can be attributed to the umbrella mode of the NH_3^+ group of cysteine calculated at 1446, 1493 and 1492 cm^{-1} for **cSz-1**, **-2** and **-3**, respectively, and confirms that cysteine mainly exists as a zwitterion in its interaction with cisplatin. IRMPD signals in the lowest part of the explored IR range are well simulated by the umbrella modes of the ammonia ligand and the OH bending modes calculated for the whole set of selected isomers (see Table S2). Isomers pertaining to the **cN** and **cSH** families are not likely to play an important role in the assayed ion population. In fact, the lowest energy structures **cN-1** and **cS-1** present important spectroscopic features, particularly at 1453 cm^{-1} and 3563 cm^{-1} in the calculated spectra of **cN-1** and **cS-1**, respectively, that are missing in the experimental IRMPD spectrum. Also, their high relative free energies (>25 kJ mol^{-1}) do not justify their participation in the sampled ion population.

3.3 IRMPD spectroscopy and structure of the cis-$[PtCl(NH_3)_2(H_2O)(Cys)]^+$ *encounter complex*

The displacement of a water molecule from *cis*-$[PtCl(NH_3)_2(H_2O)]^+$ occurs through the formation of a complex where a ligand, such as cysteine, enters the second coordination sphere of Pt,

interacting with *cis*-$[PtCl(NH_3)_2(H_2O)]^+$ by means of non-covalent interactions in a so-called encounter complex, **ec**, {*cis*-$[PtCl(NH_3)_2(H_2O)]^+$ • Cys}. Following the ligand exchange reaction, water is released from the first to the second coordination sphere leading to the product adduct, **pa**, {*cis*-$[PtCl(NH_3)_2(Cys)]^+$ • H_2O}. Geometry optimization calculations of **ec** and **pa** complexes were performed, and the lowest lying structures are displayed in Fig. 3.

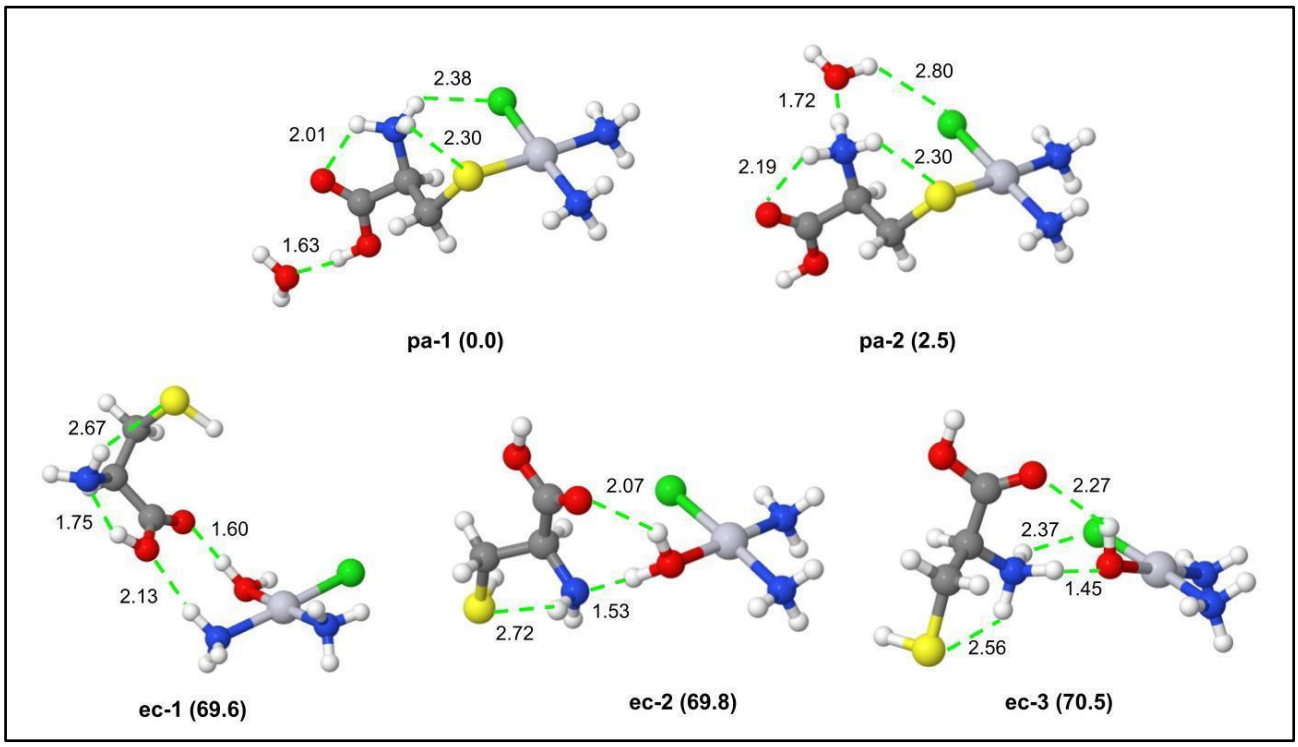

Fig. 3. Optimized geometries of the most stable conformers of the *cis*-$[PtCl(NH_3)_2(H_2O)(Cys)]^+$ ion, computed in gas phase at B3LYP/BS1 level of theory. Relative free energies referred to **pa-1** are reported in parenthesis in kJ mol^{-1}. Hydrogen bond distances (Å) are indicated by green dashed lines.

The lowest energy structure of the non-covalent adduct is represented by **pa-1**, characterized by a S-Pt bond and by a protonated amino group. The H bonds pattern is rather similar to that found for **cSz-1** with $r(NH_2\text{-}H^+\cdots O{=}C)$, $r(NH_2\text{-}H^+\cdots S)$ and $r(NH_2\text{-}H^+\cdots Cl)$ of 2.01, 2.30 and 2.38 Å, respectively. The water molecule in the external coordination sphere is H bond acceptor to the *cis* carboxylic function. In **pa-2** (2.5 kJ mol^{-1}), water interacts with α-NH_3^+ and with Cl via H bond

contacts. The intramolecular hydrogen bonds are the same as described for **pa-1**. The most stable structure of the encounter complex {*cis*-$[PtCl(NH_3)_2(H_2O)]^+$ • Cys} is represented by **ec-1** where the COOH function of cysteine in the second coordination sphere is in *trans* configuration and acts as H bond acceptor allowing the formation of two H bonds with water and NH_3 ligands. At similar relative free energy, cysteine can interact with *cis*-$[PtCl(NH_3)_2(H_2O)]^+$ through binding via two H bonds with water by means of C=O and NH_2 acceptors. As also reported for the {*cis*-$[PtCl(NH_3)_2(H_2O)]^+$ • Met} complex [23], a proton transfer can occur in the gas phase from H_2O(Pt) to the α-NH_2 group leading to a {*cis*-$[PtCl(NH_3)_2(HO)]$ • $CysH^+$} isomer, such as **ec-3**, that is only 0.7 kJ mol^{-1} higher in energy than **ec-2**.

The reported lowest energy structures are in good agreement with a computational study focused on *cis*-$[PtCl(NH_3)_2(H_2O)(Cys)]^+$ [62]. Other conformers/isomers of **pa** and **ec** adducts are displayed in Fig. S12-S13 and S14-S15, respectively, while the relative free energy values are reported in Table S3 and Table S4. The IRMPD spectrum of *cis*-$[PtCl(NH_3)_2(H_2O)(Cys)]^+$ is shown in Fig. 4 and compared with calculated IR spectra of selected isomers.

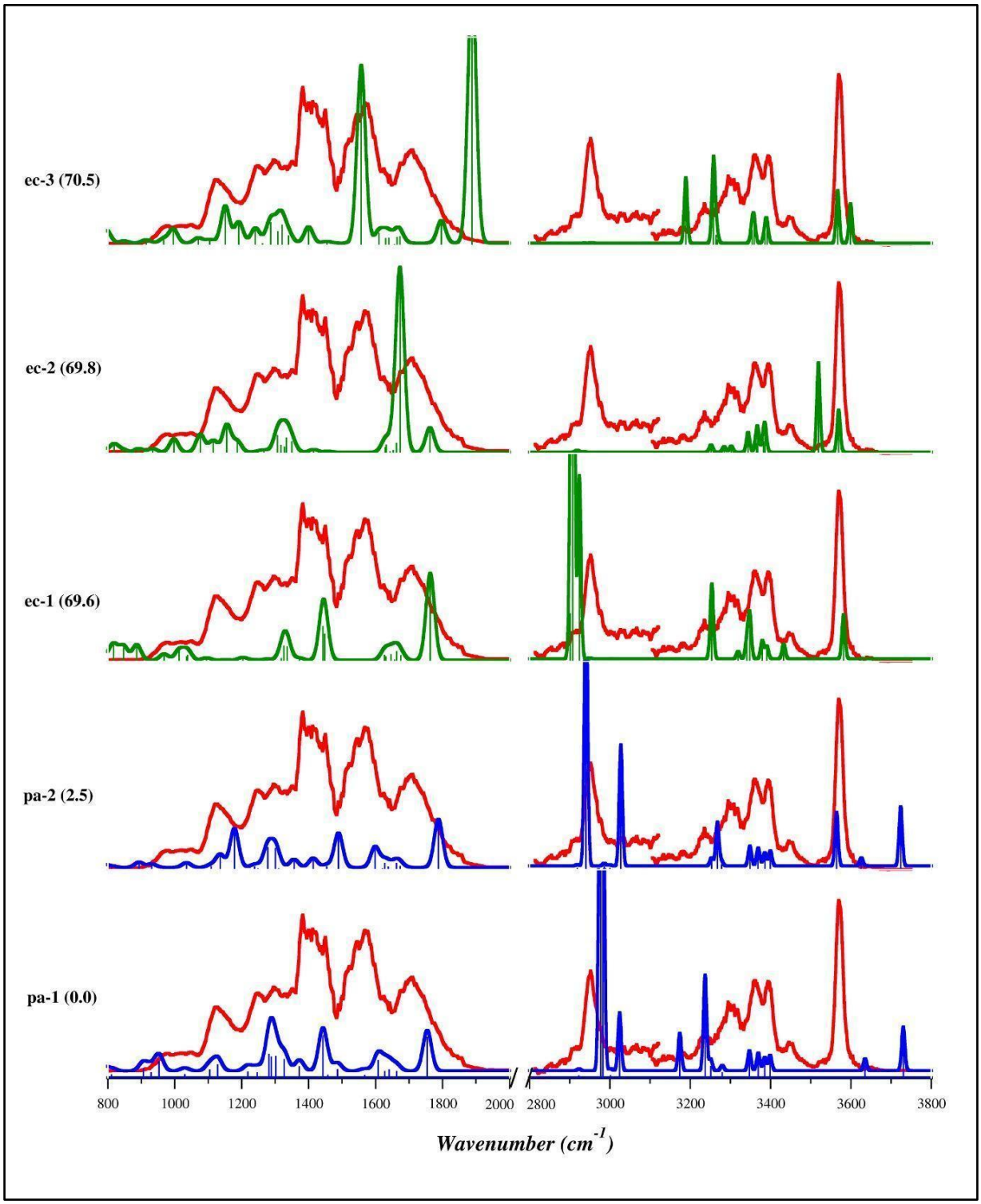

Fig. 4. IRMPD spectrum (red profile) and calculated harmonic IR spectra of the three lowest lying conformers and isomers of **pa**, {*cis*-$[PtCl(NH_3)_2(Cys)]^+ \bullet H_2O$}, (blue profiles) and **ec**, {*cis*-$[PtCl(NH_3)_2(H_2O)]^+ \bullet$ Cys}, (green profiles) ions, computed at the B3LYP/BS1 level of theory. Free energies relative to **pa-1** are reported in brackets (kJ mol^{-1}).

As reported in Section 3.1, photofragmentation yields both water and cysteine loss in a comparable ratio as already observed for other *cis*-$[PtCl(NH_3)_2(H_2O)(L)]^+$ complexes [23,38,39]. Fig. S16 shows that both dissociation paths display the same profile as a function of the photon energy, assessing that the observed fragmentation channels belong to the same species. Comparison of experimental and theoretical spectra points to the presence of a mixture of conformers pertaining to the **ec** family, in particular the lowest lying **ec-1**, **ec-2** and **ec-3** (Fig. 3 and Table S5). Spectroscopy thus confirms that we are assaying the encounter complex of *cis*-$[PtCl(NH_3)_2(H_2O)]^+$ and neutral cysteine, namely {*cis*-$[PtCl(NH_3)_2(H_2O)]^+$·(Cys)} (**ec-n** structures), as opposed to the water-solvated substitution complex {*cis*-$[PtCl(NH_3)_2(Cys)]^+$·(H_2O)} (**pa-n** structures). The IRMPD spectrum in the XH stretching range is characterized by a strong absorption at 3570 cm^{-1} accompanied by minor shoulders at 3600 and 3527 cm^{-1}. The proposed predominant contribution of **ec-1**, **ec-2** and **ec-3** in the gas-phase population can well reproduce the following features: i) the main band at 3570 cm^{-1} is attributable to a combination of the stretching modes of the free OH of water in **ec-1** (3582 cm^{-1}), and the carboxylic OH in **ec-2** and **ec-3** (3570 and 3568 cm^{-1}, respectively); ii) the free OH stretching of water in **ec-2** at 3518 cm^{-1} simulates the small band at 3527 cm^{-1}; and iii) the higher wavenumber shoulder at 3600 cm^{-1} can be attributed to the stretching of the Pt-bound OH calculated at 3598 cm^{-1} in **ec-3**. Eventually, the absence of any experimental band above 3600 cm^{-1} confirms that structures of the **pa** family are not represented in the gas-phase population being the asymmetric stretching of water a characteristic absorption of these isomers at ca. 3750 cm^{-1} (Fig. 3 and Fig. S17-S20). IRMPD bands between 3450 and 3200 cm^{-1} can be interpreted by a combination of the several NH_3 stretching modes calculated in this spectroscopic range for all the selected structures (Table S5). A band at 2947 cm^{-1} suggests the predominant presence of **ec-1** which shows a strong absorption related to the coupled OH stretching modes of both water and cysteine at 2923 cm^{-1} and 2906 cm^{-1}. In the

fingerprint range the broad band centered at 1710 cm^{-1} supposedly contains a combination of CO stretching modes (1763, 1762 and 1796 cm^{-1} for **ec-1**, **ec-2** and **ec-3**, respectively) and H_2O scissoring modes (1662 and 1673 cm^{-1} for **ec-1** and **ec-2**, respectively). The massive NH bending of the protonated cysteine amino group, calculated at 1888 cm^{-1} for **ec-3**, is probably not observable due to the combined effect of the lower laser power at this frequency close to the terminus of the inspected range (795 mW at 1900 cm^{-1}, as compared to 1460 mW at 1600 cm^{-1}) and the arguably high anharmonicity of the mode, which can broaden and reduce the activity of the IRMPD band [20,21,48,63-65]. Conformer **ec-3** accounts for the 1570 cm^{-1} IRMPD band due to the umbrella mode of cysteine protonated on the amino group (1557 cm^{-1}). Experimental bands in the lower frequency range can be attributed to a combination of the ammonia ligand umbrella modes and of the cysteine OH bending modes pertaining to this range for all the selected isomers (Table S5). The calculated harmonic IR spectra of other optimized **ec** conformers and isomers are shown in Fig. S21-S24.

Spectroscopy confirms that ESI-MS allows the isolation and characterization of the encounter complex {*cis*-$[PtCl(NH_3)_2(H_2O)]^+$·(Cys)}, which evolves to the substitution product upon activation in the gas-phase. In the forthcoming section the energetics of this reaction will be discussed in more detail and correlated to the fragmentation pattern reported in Section 3.1 with the aid of DFT calculations of its energy profile.

3.4 Activation of the bare encounter complex, correlation with the PES for ligand substitution

To clarify the role of the encounter complex in the framework of the energy profile of the substitution reaction between *cis*-$[PtCl(NH_3)_2(H_2O)]^+$ and cysteine, calculations at the DFT level were performed. Theoretical evidence can indeed provide the basis for explaining the fragmentation behavior of **ec**. To estimate the activation energy of the water substitution reaction (Scheme 2) from the encounter complex to the product adduct, transition-state optimization

and subsequent IRC calculations were performed at the B3LYP/BS1 level of theory. As shown in Fig. S25, the optimized TS structure is characterized by S-Pt and H_2O-Pt bond distances equal to 2.81 and 2.44 Å, respectively, while the H_2O-Pt-S bond angle is 73.8°. The leaving water molecule is linked by a hydrogen bond with NH_2, which stabilizes the TS structure as also found in the TS of the similar reaction of *cis*-$[PtCl(NH_3)_2(H_2O)(Met)]^+$ [23].

$$\{\textit{cis}\text{-}[PtCl(NH_3)_2(H_2O)]^+\cdot(L)\} \xrightarrow{\textbf{ec}} TS \longrightarrow \{\textit{cis}\text{-}[PtCl(NH_3)_2(L)]^+\cdot(H_2O)\} \xrightarrow{\textbf{pa}} \textit{cis}\text{-}[PtCl(NH_3)_2(L)]^+ \quad (-H_2O)$$

Scheme 2. Substitution reaction of hydrolyzed cisplatin by a ligand (L).

The results of the IRC calculations (Fig. S26) indicate that cysteine, located in the second coordination sphere of platinum, is first involved in two hydrogen bonds with one of the ammonia ligands and with water by means of SH and NH_2 acceptors, respectively (Fig. S27). Then, S...NH_3(Pt) H bond breaks to give the TS. After S-Pt bond formation (Fig. S27), the leaving water molecule interacts as a H bond acceptor with the ammonia ligand while maintaining a contact with α-NH_2.

Fig. 5 shows the calculated energy profile for the substitution reaction of *cis*-$[PtCl(NH_3)_2(H_2O)]^+$ with cysteine. Enthalpy values are obtained from the enthalpy corrected electronic energy of the lowest lying encounter complex structure, **ec-1**. The ωB97X-D/BS1//B3LYP/BS1 level of theory was used to allow the comparison of thermodynamic data with previously reported energy profiles for similar reactions [23,38,39].

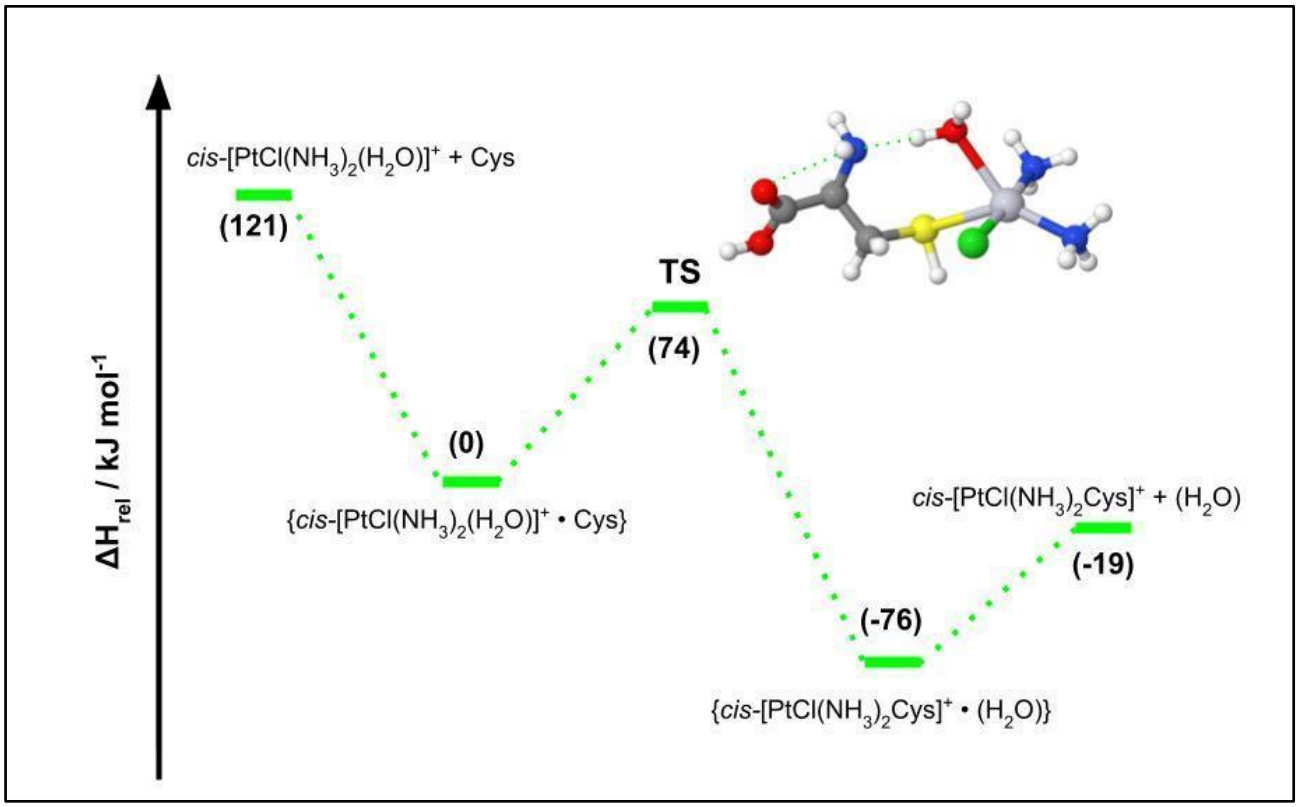

Fig. 5. Energy profile for the reaction of *cis*-$[PtCl(NH_3)_2(H_2O)]^+$ with cysteine. Relative enthalpy values at 298 K (in parentheses), computed at the ωB97X-D/BS1//B3LYP/BS1 level of theory, are reported in kJ mol^{-1}. The transition state geometry (TS) is also shown.

In agreement with the reaction pattern of *cis*-$[PtCl(NH_3)_2(H_2O)]^+$ with methionine [23] and with smaller systems mimicking biological ligands [38,39], the encounter complex lies in the first potential energy well, which allows it to be observed, mass-isolated and characterized. The underlying notion is that energy imparted to the complex during the ESI process, while large enough to remove the water solvent from {*cis*-$[PtCl(NH_3)_2(Cys)]^+ \cdot (H_2O)$}, does not permit to overcome the energy barrier of the pentacoordinated TS (74 kJ mol^{-1}) for the substitution process nor the threshold for backward cleavage of cysteine (121 kJ mol^{-1}). The encounter complex is therefore kinetically trapped in the transfer from solution to the gas-phase. The overall substitution process is exoergonic in agreement with the thiophilic character of Pt(II) and the abundant evidence pointing to the coordination of cisplatin in proteins with sulfur-containing

amino acids [8-19]. The reaction product presents a thiolate group bound to Pt(II), as highlighted in Section 3.2, while in **ec-1** cysteine in neutral form thiolate is non-covalently bound to positively charged *cis*-$[PtCl(NH_3)_2(H_2O)]^+$. The question arises on whether the proton transfer from the -SH to the amino group of cysteine occurs before or after the TS formation. Starting from the proposed TS (Fig. S25), IRC leads to a higher energy structure with cysteine still in neutral form, when compared to **pa-1** (46.9 kJ mol^{-1}, see Fig. S27). Therefore, proton transfer is likely to occur in a fast step shortly before the formation of **pa-1** and the final dissociation of water. The required energy can be inferred to be in the range of 10 kJ mol^{-1} as in the case of the substitution product (Fig. S7). An alternative transition state bearing the proton on the cysteine amino group was also calculated (Fig. S28) but is characterized by a higher energy barrier (111 kJ mol^{-1}), strengthening the hypothesis that the proton transfer does occur after the water substitution reaction. Thermodynamic data can also be used to explain the peculiar **ec** gas-phase reactivity. In fact, the dissociation process involving water loss was found to increase with respect to the ligand loss as the energy difference between the TS and the incoming ligand back dissociation decreases. In the exemplary case of methionine, when the {*cis*-$[PtCl(NH_3)_2(H_2O)]^+$·(Met)} complex is activated, the water loss dissociation path was found to account for 97% of the total fragmentation, while methionine loss was the 3%, in agreement with the high energy difference of 70 kJ mol^{-1} between the direct cleavage of methionine and the TS leading to the substitution product [23]. The dissociation behavior of {*cis*-$[PtCl(NH_3)_2(H_2O)]^+$·(Cys)} is quite different: the observed 25% fraction of water loss places the ligand substitution reactivity of the cysteine complex in between pyridine (5% water loss) and 4-methylimidazole (82% water loss) [38]. For these compounds the calculated energy difference between the threshold for back dissociation and the TS for ligand substitution is 43 and 65 kJ mol^{-1}, respectively. Therefore, the 47 kJ mol^{-1} difference calculated in the case of cysteine well accounts for the experimental findings.

Conclusions

Cisplatin readily interacts with cysteine in aqueous solution producing several ionic species. Among them, the encounter complex {*cis*-$[PtCl(NH_3)_2(H_2O)]^+$·(Cys)} and the substitution product *cis*-$[PtCl(NH_3)_2(Cys)]^+$ play key roles in the reaction of cisplatin with cysteine. They lie in the path which leads to the formation of the final substitution product starting from hydrolyzed cisplatin and neutral cysteine. These intermediates were mass-selected and characterized using IRMPD spectroscopy and DFT calculations. {*cis*-$[PtCl(NH_3)_2(H_2O)]^+$·(Cys)} presents cysteine non-covalently bound to the aqua and ammonia ligands. Activation of the mass-isolated complex in the gas-phase produces competitive dissociation of either cysteine or water, thus suggesting that water is substituted by cysteine in the Pt coordination sphere upon activation. Indeed, this is possible considering that Pt(II) complexes present a square-planar geometry which allows the substitution process through a concerted mechanism. The pentacoordinated transition state which leads to the water loss was characterized by DFT calculations and its energy compared to the threshold for the cysteine back dissociation from the encounter complex. The resulting 47 kJ mol^{-1} enthalpy difference is in line with the observed 75% fraction of water dissociation, following the same behavior reported for hydrolyzed cisplatin with methionine and other model ligands. The weight of the water loss channel along the sampled incoming ligands follows the trend: methionine > urea ≈ dimethylacetamide ≈ acetamide > trimethylphosphate > (5)-methylimidazole > cysteine > pyridine and is well simulated by the thermodynamic data. Table S6 collects the values reported for the different ligands and compares them with calculated energies and reaction efficiencies for the substitution reaction (as available for volatile neutrals). Cysteine appears to be significantly less reactive than methionine whose encounter complex leads to ca. 97% water loss when activated, though having a comparable activation barrier. The reason is thus to be found in the energy released in the association process, namely 121 and 141 kJ mol^{-1} for *cis*-$[PtCl(NH_3)_2(H_2O)]^+$

and cysteine or methionine, respectively, making the reaction faster for methionine, and determining a higher dissociation yield ratio. The structural characterization of the final product *cis*-$[PtCl(NH_3)_2(Cys)]^+$ has shown several conformers to participate in the assayed gas-phase population. However, a common trait is cysteine binding to Pt(II) through the thiolate functionality while the amino group is protonated. Binding to platinum increases the acidity of cysteine SH group, which otherwise is not the main deprotonation site in bare cysteine.

ESI-MS coupled to IRMPD spectroscopy confirms its potential for the characterization of reactive intermediates of bioinorganic relevance. In addition, the possibility to obtain semiquantitative data about the efficiency of substitution reactions in aquated cisplatin complexes through the encounter complex gas-phase activation is assessed.

Acknowledgment

This work was funded by the Italian Ministry for University and Research - Dipartimenti di Eccellenza - L. 232/2016, and by the European Union's Horizon 2020 research and innovation programme under grant agreement No 731077 (EU_FT-ICR_MS) and grant agreement No 730872 (CALIPSO plus). We are grateful to all the CLIO team for their valuable assistance.

References

[1] Cisplatin: Chemistry and Biochemistry of a Leading Anticancer Drug; Lippert, B., Ed.; Wiley, 1999.

[2] E.R. Jamieson, S.J. Lippard, Structure, Recognition, and Processing of Cisplatin−DNA Adducts, Chem. Rev. 99 (1999) 2467− 2498,

[3] E. Wong, C.M. Giandomenico, Current Status of Platinum- Based Antitumor Drugs, Chem. Rev. 99 (1999) 2451−2466, https://doi.org/10.1021/cr980420v .

[4] M.A. Fuertes, C. Alonso, J.M. Pérez, Biochemical Modulation of Cisplatin Mechanisms of Action: Enhancement of Antitumor Activity and Circumvention of Drug Resistance, Chem. Rev. 103 (2003) 645−662, https://doi.org/10.1021/cr020010d.

[5] A.V. Klein, T.W. Hambley, Platinum Drug Distribution in Cancer Cells and Tumors, Chem. Rev. 109 (2009) 4911−4920, https://doi.org/10.1021/cr9001066

[6] S. Dasari, P.B. Tchounwou, Cisplatin in Cancer Therapy: Molecular Mechanisms of Action, Eur. J. Pharmacol. 740 (2014) 364− 378, https://doi.org/10.1016/j.ejphar.2014.07.025 .

[7] A. Casini, J. Reedijk, Interactions of Anticancer Pt Compounds with Proteins: An Overlooked Topic in Medicinal Inorganic Chemistry? Chem. Sci. 3 (2012) 3135, https://doi.org/10.1039/C2SC20627G.

[8] L. Messori, A. Merlino, Cisplatin Binding to Proteins: Molecular Structure of the Ribonuclease A Adduct, Inorg. Chem. 53 (2014) 3929−3931, https://doi.org/10.1021/ic500360f.

[9] C.M. Sze, G.N. Khairallah, Z. Xiao, P.S. Donnelly, R.A.J. O'Hair, A.G. Wedd, Interaction of Cisplatin and Analogues with a Met-Rich Protein Site, J. Biol. Inorg. Chem. 14 (2009) 163−165, https://doi.org/10.1007/s00775-008-0452-x.

[10] J. Reedijk, Why Does Cisplatin Reach Guanine-N7 with Competing S-Donor Ligands Available in the Cell? Chem. Rev. 99 (1999) 2499−2510,

[11] K.M. Williams, C. Rowan, J. Mitchell, Effect of Amine Ligand Bulk on the Interaction of Methionine with Platinum(II) Diamine Complexes, Inorg. Chem. 43 (2004) 1190−1196, https://doi.org/10.1021/ic035212m .

[12] D.V. Deubel, Factors Governing the Kinetic Competition of Nitrogen and Sulfur Ligands in Cisplatin Binding to Biological Targets, J. Am. Chem. Soc. 126 (2004) 5999−6004, https://doi.org/10.1021/ja0499602.

[13] O. Vrana, V Brabec, L-Methionine Inhibits Reaction of DNA with Anticancer Cis-Diamminedichloroplatinum(II), Biochemistry 41 (2002) 10994−10999.

[14] T. Soldatović, Ž.D. Bugarčić, Study of the Reactions between Platinum(II) Complexes and l-Methionine in the Presence and Absence of 5′-GMP, J. Inorg. Biochem. 99 (2005) 1472−1479, https://doi.org/10.1016/j.jinorgbio.2005.04.005.

[15] A.I. Ivanov, J. Christodoulou, J.A. Parkinson, K.J. Barnham, A. Tucker, J. Woodrow, P.J. Sadler, Cisplatin Binding Sites on Human Albumin, J. Biol. Chem. 273 (1998) 14721−14730, https://doi.org/10.1074/jbc.273.24.14721.

[16] H. Li, Y. Zhao, H.I.A. Phillips, Y. Qi, T.Y. Lin, P.J. Sadler, P.B. O'Connor, Mass Spectrometry Evidence for Cisplatin as a Protein Cross-Linking Reagent, Anal. Chem. 83 (2011) 5369−5376, https://doi.org/10.1021/ac200861k.

[17] H. Li, J.R. Snelling, M.P. Barrow, J.H. Scrivens, P.J. Sadler, P.B. O'Connor, Mass Spectrometric Strategies to Improve the Identification of Pt(II)-Modification Sites on Peptides and Proteins, J. Am. Soc. Mass Spectrom. 25 (2014) 1217−1227, https://doi.org/10.1007/s13361-014-0877-0.

[18] F. Arnesano, S. Scintilla, G. Natile, Interaction between Platinum Complexes and a Methionine Motif Found in Copper Transport Proteins, Angew. Chem., Int. Ed. 46 (2007) 9062−9064, https://doi.org/10.1002/ange.200703271.

[19] Ž.D. Bugarčić, J. Bogojeski, B. Petrović, S. Hochreuther, R. van Eldik, Mechanistic Studies on the Reactions of Platinum(II) Complexes with Nitrogen- and Sulfur-Donor Biomolecules, Dalton Trans. 41 (2012) 12329, https://doi.org/10.1039/C2DT31045G

[20] R. Paciotti, D. Corinti, A. De Petris, A. Ciavardini, S. Piccirillo, C. Coletti, N. Re, P. Maitre, B. Bellina, P. Barran, B. Chiavarino, M. Elisa Crestoni, S. Fornarini, Cisplatin and transplatin interaction with methionine: bonding motifs assayed by vibrational spectroscopy in the isolated ionic complexes, Phys. Chem. Chem. Phys. 19 (2017) 26697–26707, https://doi.org/10.1039/C7CP05203K.

[21] D. Corinti, A. De Petris, C. Coletti, N. Re, B. Chiavarino, M.E. Crestoni, S. Fornarini, Cisplatin Primary Complex with l-Histidine Target Revealed by IR Multiple Photon Dissociation (IRMPD) Spectroscopy, ChemPhysChem. 18 (2017) 318–325, https://doi.org/10.1002/cphc.201601172

[22] D. Corinti, R. Paciotti, N. Re, C. Coletti, B. Chiavarino, M.E. Crestoni, S. Fornarini, Binding motifs of cisplatin interaction with simple biomolecules and aminoacid targets probed by IR ion spectroscopy, Pure Appl. Chem. 92 (2020) 3–13, https://doi.org/10.1515/pac-2019-0110.

[23] R. Paciotti, D. Corinti, P. Maitre, C. Coletti, N. Re, B. Chiavarino, M.E. Crestoni, S. Fornarini, From Preassociation to Chelation: A Survey of Cisplatin Interaction with Methionine at Molecular Level by IR Ion Spectroscopy and Computations, J. Am. Soc. Mass Spectrom. 32 (2021) 2206–2217, https://doi.org/10.1021/jasms.1c00152.

[24] B. Chiavarino, M.E. Crestoni, S. Fornarini, D. Scuderi, J.-Y. Salpin, Interaction of cisplatin with adenine and guanine: A combined IRMPD, MS/MS, and theoretical study, J. Am. Chem. Soc. 135 (2013) 1445–1455, https://doi.org/10.1021/ja309857d.

[25] B. Chiavarino, M.E. Crestoni, S. Fornarini, D. Scuderi, J.-Y. Salpin, Interaction of Cisplatin with 5′-dGMP: A Combined IRMPD and Theoretical Study, Inorg. Chem. 54 (2015) 3513–3522, https://doi.org/10.1021/acs.inorgchem.5b00070.

[26] C.C. He, B. Kimutai, X. Bao, L. Hamlow, Y. Zhu, S.F. Strobehn, J. Gao, G. Berden, J. Oomens, C.S. Chow, M.T. Rodgers, Evaluation of Hybrid Theoretical Approaches for Structural Determination of a Glycine-Linked Cisplatin Derivative via Infrared Multiple Photon Dissociation (IRMPD) Action Spectroscopy, J. Phys. Chem. A. 119 (2015) 10980–10987, https://doi.org/10.1021/acs.jpca.5b08181.

[27] B. Chiavarino, M.E. Crestoni, S. Fornarini, D. Scuderi, J.-Y. Salpin, Undervalued N3 Coordination Revealed in the Cisplatin Complex with 2′-Deoxyadenosine-5′-monophosphate by a Combined IRMPD and Theoretical Study, Inorg. Chem. 56 (2017) 8793–8801, https://doi.org/10.1021/acs.inorgchem.7b00570.

[28] D. Corinti, M.E. Crestoni, B. Chiavarino, S. Fornarini, D. Scuderi, J.-Y. Salpin, Insights into Cisplatin Binding to Uracil and Thiouracils from IRMPD Spectroscopy and Tandem Mass Spectrometry, J. Am. Soc. Mass Spectrom. 31 (2020) 946–960, doi:10.1021/jasms.0c00006.

[29] C.C. He, L.A. Hamlow, B. Kimutai, H.A. Roy, Z.J. Devereaux, N.A. Cunningham, J. Martens, G. Berden, J. Oomens, C.S. Chow, M.T. Rodgers, Structural determination of arginine-linked cisplatin complexes via IRMPD action spectroscopy: arginine binds to platinum via NO − binding mode, Phys. Chem. Chem. Phys. 23 (2021) 21959–21971, doi:10.1039/D1CP03407C.

[30] L. MacAleese, P. Maître, Infrared Spectroscopy of Organo-metallic Ions in the Gas Phase: From Model to Real World Complexes, Mass Spectrom. Rev. 26 (2007) 583−605, https://doi.org/10.1002/mas.20138.

[31] L. Jašíková, J. Roithová, Infrared Multiphoton Dissociation Spectroscopy with Free-Electron Lasers: On the Road from Small Molecules to Biomolecules, Chem. - Eur. J. 24 (2018) 3374−3390, https://doi.org/10.1002/chem.201705692.

[32] J.R. Eyler, Infrared Multiple Photon Dissociation Spectroscopy of Ions in Penning Traps. Mass Spectrom. Rev. 28 (2009) 448−467, https://doi.org/10.1002/mas.20217.

[33] T.D. Fridgen, Infrared Consequence Spectroscopy of Gaseous Protonated and Metal Ion Cationized Complexes. Mass Spectrom. Rev. 28 (2009) 586−607, https://doi.org/10.1002/mas.20224.

[34] N.C. Polfer, J. Oomens, Vibrational Spectroscopy of Bare and Solvated Ionic Complexes of Biological Relevance, Mass Spectrom. Rev. 28 (2009) 468−494, https://doi.org/10.1002/mas.20215.

[35] M.S. Davies, S.J. Berners-Price, T.W. Hambley, Slowing of Cisplatin Aquation in the Presence of DNA but Not in the Presence of Phosphate: Improved Understanding of Sequence Selectivity and the Roles of Monoaquated and Diaquated Species in the Binding of Cisplatin to DNA, Inorg. Chem. 39 (2000) 5603–5613, https://doi.org/10.1021/ic000847w.

[36] J. Kozelka, Molecular origin of the sequence-dependent kinetics of reactions between cisplatin derivatives and DNA, Inorg. Chim. Acta 362 (2009) 651–668, https://doi.org/10.1016/j.ica.2008.04.024.

[37] D. Corinti, C. Coletti, N. Re, S. Piccirillo, M. Giampà, M.E. Crestoni, S. Fornarini, Hydrolysis of cis- and transplatin: structure and reactivity of the aqua complexes in a solvent free environment, RSC Adv. 7 (2017) 15877–15884, doi:10.1039/C7RA01182B.

[38] D. Corinti, C. Coletti, N. Re, B. Chiavarino, M.E. Crestoni, S. Fornarini, Cisplatin Binding to Biological Ligands Revealed at the Encounter Complex Level by IR Action Spectroscopy, Chem. - A Eur. J. 22 (2016) 3794–3803, doi:10.1002/chem.201504521.

[39] D. Corinti, C. Coletti, N. Re, R. Paciotti, P. Maître, B. Chiavarino, M.E. Crestoni, S. Fornarini, Short-lived intermediates (encounter complexes) in cisplatin ligand exchange elucidated by infrared ion spectroscopy, Int. J. Mass Spectrom. 435 (2019) 7–17, doi:10.1016/j.ijms.2018.10.012.

[40] D.T. Richens, Ligand Substitution Reactions at Inorganic Centers. Chem. Rev. 105 (2005) 1961−2002, https://doi.org/10.1021/cr030705u.

[41] M. Eigen, Fast Elementary Steps in Chemical Reaction Mechanisms, Pure Appl. Chem. 6 (1963) 97−116, https://doi.org/10.1351/pac196306010097.

[42] C.E. Housecroft, A.G. Sharpe, Inorganic Chemistry, 2nd ed.; Pearson Education, 2005.

[43] J. Burgess, Ions in Solution. Basic Principles of Chemical Interactions, 2nd ed.; Woodhead Publishing, 2011.

[44] D. Corinti, M.E. Crestoni, S. Fornarini, E. Dabbish, E. Sicilia, E. Gabano, E. Perin, D. Osella, A multi-methodological inquiry of the behavior of cisplatin-based Pt(IV) derivatives in the presence of bioreductants with a focus on the isolated encounter complexes, JBIC J. Biol. Inorg. Chem. 25 (2020) 655–670, doi:10.1007/s00775-020-01789-w.

[45] M. Citir, E.M.S. Stennett, J. Oomens, J.D. Steill, M.T. Rodgers, P.B. Armentrout, Infrared multiple photon dissociation spectroscopy of cationized cysteine: Effects of metal cation size on gas-phase conformation, Int. J. Mass Spectrom. 297 (2010) 9–17. doi:10.1016/j.ijms.2010.04.009.

[46] R.A. Coates, C.P. McNary, G.C. Boles, G. Berden, J. Oomens, P.B. Armentrout, Structural characterization of gas-phase cysteine and cysteine methyl ester complexes with zinc and

cadmium dications by infrared multiple photon dissociation spectroscopy, Phys. Chem. Chem. Phys. 17 (2015) 25799–25808, doi:10.1039/C5CP01500F.

[47] C. Ieritano, P.J.J. Carr, M. Hasan, M. Burt, R.A. Marta, V. Steinmetz, E. Fillion, T.B. McMahon, W. Scott Hopkins, The structures and properties of proton-and alkali-bound cysteine dimers, Phys. Chem. Chem. Phys. 18 (2016) 4704–4710.,doi:10.1039/c5cp07414b.

[48] J. Oomens, J.D. Steill, B. Redlich, Gas-Phase IR Spectroscopy of Deprotonated Amino Acids, J. Am. Chem. Soc. 131 (2009) 4310−4319, https://doi.org/10.1021/ja807615v.

[49] J.D. Steill, J. Szczepanski, J. Oomens, J.R. Eyler, A. Brajter-Toth, Structural characterization by infrared multiple photon dissociation spectroscopy of protonated gas-phase ions obtained by electrospray ionization of cysteine and dopamine, Anal. Bioanal. Chem. 399 (2011) 2463–2473. doi:10.1007/s00216-010-4582-y.

[50] R.K. Sinha, P. Maître, S. Piccirillo, B. Chiavarino, M.E. Crestoni, S. Fornarini, Cysteine radical cation: A distonic structure probed by gas phase IR spectroscopy, Phys. Chem. Chem. Phys. 12 (2010) 9794, doi:10.1039/c003576a.

[51] M. Lesslie, J.K.C. Lau, J.T. Lawler, K.W.M. Siu, V. Steinmetz, P. Maître, A.C. Hopkinson, V. Ryzhov, Cysteine Radical/Metal Ion Adducts: A Gas-Phase Structural Elucidation and Reactivity Study, Chempluschem. 81 (2016) 444–452, doi:10.1002/cplu.201500558.

[52] F. Lanucara, B. Chiavarino, M.E. Crestoni, D. Scuderi, R.K. Sinha, P. Maître, S. Fornarini, S-Nitrosation of Cysteine as Evidenced by IRMPD Spectroscopy, Int. J. Mass Spectrom. 330–332 (2012) 160–167, https://doi.org/10.1016/j.ijms.2012.07.003.

[53] C. Jocelyn, Biochemistry of the SH Group, Vol. 270, Academic Press, London, 1972.

[54] J. Stubbe, W.A. van der Donk, Protein Radicals in Enzyme Catalysis, Chem. Rev. 98 (1998) 705–762, doi:10.1021/cr9400875.

[55] M.H. Stipanuk, J.E. Dominy, J.-I. Lee, R.M. Coloso, Mammalian Cysteine Metabolism: New Insights into Regulation of Cysteine Metabolism, J. Nutr. 136 (2006) 1652S-1659S, doi:10.1093/jn/136.6.1652S.

[56] J.M. Bakker, T. Besson, J. Lemaire, D. Scuderi, P. Maître, Gas-Phase Structure of a π-Allyl−Palladium Complex: Efficient Infrared Spectroscopy in a 7 T Fourier Transform Mass Spectrometer J. Phys. Chem. A 2007, 111, 13415-13424, https://doi.org/10.1021/jp074935e.

[57] R.K. Sinha, P. Maître, S. Piccirillo, B. Chiavarino, M. E. Crestoni, S. Fornarini, Phys. Chem. Chem. Phys. 2010, 12, 9794-9800.

[58] J. S. Prell, J. T. O'Brien, E. R. Williams, IRPD Spectroscopy and Ensemble Measurements: Effects of Different Data Acquisition and Analysis Methods J. Am. Soc. Mass Spectrom. 21 (2010) 800-809, https://doi.org/10.1016/j.jasms.2010.01.010.

[59] P. Pracht, F. Bohle, S. Grimme, Automated exploration of the low-energy chemical space with fast quantum chemical methods, Phys. Chem. Chem. Phys. 22 (2020) 7169-7192, https://doi.org/10.1039/C9CP06869D.

[60] M.J. Frisch, G.W. Trucks, H.B. Schlegel, G.E. Scuseria, M.A. Robb, J.R. Cheeseman, G. Scalmani, V. Barone, B. Mennucci, G.A. Petersson Gaussian 09, Revision D.01; Gaussian Inc.: Wallingford, CT, USA, 2009.

[61] E. Ataman, C. Isvoranu, J.N. Andersen, J. Schnadt, K. Schulte, Unconventional zwitterionic state of l-cysteine, J. Phys. Chem. Lett. 2 (2011) 1677–1681. doi:10.1021/jz2006918.

[62] T. Zimmermann, J.V. Burda, Cisplatin interaction with amino acids cysteine and methionine from gas phase to solutions with constant pH, Interdiscip Sci Comput Life Sci 2 (2010) 98–114, https://doi.org/10.1007/s12539-010-0094-x.

[63] D. Corinti, B. Chiavarino, M. Spano, A. Tintaru, S. Fornarini, M.E. Crestoni, Molecular Basis for the Remarkably Different Gas-Phase Behavior of Deprotonated Thyroid Hormones Triiodothyronine (T3) and Reverse Triiodothyronine (rT3): A Clue for Their Discrimination? Anal. Chem. 93 (2021) 14869–14877, https://doi.org/10.1021/acs.analchem.1c03892.

[64] R. Paciotti, C. Coletti, N. Re, D. Scuderi, B. Chiavarino, S. Fornarini, M. E. Crestoni, Serine O-sulfation probed by IRMPD spectroscopy, Phys. Chem. Chem. Phys. 17 (2015) 25891–25904, https://doi.org/10.1039/C5CP01409C.

[65] D. Corinti, M.E. Crestoni, S. Fornarini, M. Pieper, K. Niehaus, M. Giampà, An integrated approach to study novel properties of a MALDI matrix (4-maleicanhydridoproton sponge) for MS imaging analyses, Anal. Bioanal. Chem. 411 (2019) 953–964. doi:10.1007/s00216-018-1531-7.